Journal of Physics: Conference Series **3089** (2025) 012007 doi:10.1088/1742-6596/3089/1/012007

# Dirac-star-plus-wormhole configurations

**Vladimir Dzhunushaliev[1,2,3,4*], Vladimir Folomeev[1,3,4] and Nurzhan Saduyev[1]**

[1] Institute of Nuclear Physics, Almaty 050032, Kazakhstan
[2] Department of Theoretical and Nuclear Physics, Al-Farabi Kazakh National University, Almaty 050040, Kazakhstan
[3] Academician J. Jeenbaev Institute of Physics of the NAS of the Kyrgyz Republic, 265 a, Chui Street, Bishkek 720071, Kyrgyzstan
[4] International Laboratory for Theoretical Cosmology, Tomsk State University of Control Systems and Radioelectronics (TUSUR), Tomsk 634050, Russia

[*]E-mail: v.dzhunushaliev@gmail.com

**Abstract.** We study configurations consisting of a gravitating linear spinor field and a massless ghost scalar field providing a nontrivial spacetime topology. For such a mixed system, we have constructed two families of asymptotically flat asymmetric solutions describing localized configurations (Dirac stars) possessing a wormhole topology. The physical properties of such systems are completely determined by the values of the spinor frequency and the throat parameter. For a fixed value of the latter, we have compared mass curves for the two families of solutions and revealed considerable differences in their behavior and physical properties of the systems under consideration (the configurations may be regular or singular and possess one or two throats, as well as they may contain possible event horizons).

## 1. Introduction

The discovery of the accelerated expansion of the present Universe at the end of the 1990's have stimulated an active search for cosmological models describing such an acceleration [1]. Indeed, from the point of view of general relativity, the presence of the acceleration implies that the Universe should contain a special form of matter violating the energy conditions. Such form of matter was called dark energy. Its distinctive feature is the presence of negative pressure that may be even larger in magnitude (modulus) than the energy density [2]. Such form of dark energy is referred to as phantom one.

The simplest way to model the phantom dark energy is the use of the so-called ghost scalar field that has an opposite sign in front of the kinetic energy compare to ordinary scalar field used in various physical models. If such ghost scalar fields do really exist in the Universe, one can expect that, apart from their cosmological manifestation, they can also form gravitating localized configurations. In this case, such systems may be both similar to ordinary boson stars having a trivial spacetime topology and possess a nontrivial, wormhole-like topology [3-5].

At the present time such wormholes are under active investigation in different directions. One of possible options is a consideration of a situation where a wormhole, apart from a ghost scalar field, is threaded by some other extra matter [6-12]. In the present paper we study mixed systems of such type consisting of a ghost scalar field (which provides a nontrivial topology) and a Dirac field. The purpose of the present work is to study the influence that the presence of

nontrivial topology has on the structure of the corresponding solutions and characteristics of the resulting mixed Dirac-star-plus-wormhole systems. In this connection notice that Ref. [13] studies a similar system supported by a spinor field. In the present paper, we extend those solutions and compare them with new solutions found in our recent work [14].

## 2. Statement of the problem and general equations

We work within Einstein's general relativity and consider compact configurations consisting of a spinor field minimally coupled to a massless ghost scalar field. In this case, the total action can be written in the form [we use the metric signature $(+,-,-,-)$ and natural units $c = \hbar = 1$]

$$S_{\rm tot} = -\frac{1}{16\pi G}\int d^4x\sqrt{-g}R + S_{\rm sp} + S_{\rm sf}, \tag{1}$$

where $G$ is the Newtonian gravitational constant and $R$ is the scalar curvature.

The action $S_{\rm sp}$ for the spinor field $\psi$ appearing in Eq. (1) can be obtained from the Lagrangian

$$L_{\rm sp} = \frac{i}{2}\left(\bar{\psi}\gamma^\mu\psi_{;\mu} - \bar{\psi}_{;\mu}\gamma^\mu\psi\right) - \mu\bar{\psi}\psi, \tag{2}$$

where $\mu$ is the mass of the spinor field and the semicolon denotes the covariant derivative defined as $\psi_{;\mu} = [\partial_\mu + 1/8\,\omega_{ab\mu}(\gamma^a\gamma^b - \gamma^b\gamma^a)]\psi$. Here $\gamma^a$ are the Dirac matrices in the standard representation in flat space [see, e.g., Ref. [15], Eq. (7.27)]. In turn, the Dirac matrices in curved space, $\gamma^\mu = e_a{}^\mu\gamma^a$, are derived using the tetrad $e_a{}^\mu$, and $\omega_{ab\mu}$ is the spin connection [for its definition, see Ref. [15], Eq. (7.135)].

The action for the real ghost scalar field $S_{\rm sf}$ appearing in (1) can be found from the Lagrangian

$$L_{\rm sf} = -\frac{1}{2}\partial_\mu\phi\,\partial^\mu\phi.$$

Then,using the action (1), one can derive the Einstein, Dirac, and scalar field equations, respectively,

$$G_\mu^\nu \equiv R_\mu^\nu - \frac{1}{2}\delta_\mu^\nu R = 8\pi G\,T_\mu^\nu, \tag{3}$$

$$i\gamma^\mu\psi_{;\mu} - \mu\psi = 0, \tag{4}$$

$$i\bar{\psi}_{;\mu}\gamma^\mu + \mu\bar{\psi} = 0, \tag{5}$$

$$\frac{1}{\sqrt{-g}}\frac{\partial}{\partial x^\mu}\left(\sqrt{-g}g^{\mu\nu}\frac{\partial\phi}{\partial x^\nu}\right) = 0. \tag{6}$$

The equation (3) contains the energy-momentum tensor $T_\mu^\nu$, which can be represented in a symmetric form as

$$\begin{aligned} T_\mu^\nu = {} & \frac{i}{4}g^{\nu\rho}\left[\bar{\psi}\gamma_\mu\psi_{;\rho} + \bar{\psi}\gamma_\rho\psi_{;\mu} - \bar{\psi}_{;\mu}\gamma_\rho\psi - \bar{\psi}_{;\rho}\gamma_\mu\psi\right] - \delta_\mu^\nu L_{\rm sp} \\ & - \partial^\nu\phi\,\partial_\mu\phi + \frac{1}{2}\delta_\mu^\nu\,\partial^\sigma\phi\;\partial_\sigma\phi. \end{aligned} \tag{7}$$

Next, taking into account the Dirac equations (4) and (5), the Lagrangian (2) becomes $L_{\rm sp} = 0$.

Since we consider here only spherically symmetric configurations, the spacetime metric can be taken in the form

$$ds^2 = e^{A(r)}dt^2 - B(r)e^{-A(r)}[dr^2 + (r^2 + r_0^2)(d\theta^2 + \sin^2\theta d\varphi^2)], \tag{8}$$

where $e^{A(r)} = 1 - 2Gm(r)/r$, and the function $m(r)$ corresponds to the current mass of the system enclosed by a sphere with circumferential radius $r$. The parameter $r_0$ characterises the throat.

For the spinor field, we choose the following stationary Ansatz compatible with the static spherically symmetric line element (8) (see, e.g., Refs. [16, 17]):

$$\psi^T = \frac{e^{-i\Omega t}}{\sqrt{2}}\begin{pmatrix}0\\-u\end{pmatrix},\begin{pmatrix}u\\0\end{pmatrix},\begin{pmatrix}iv\sin\theta e^{-i\varphi}\\-iv\cos\theta\end{pmatrix},\begin{pmatrix}-iv\cos\theta\\-iv\sin\theta e^{i\varphi}\end{pmatrix}, \tag{9}$$

where $\Omega$ is the spinor frequency and $u(r)$ and $v(r)$ are two real functions. Each row of the Ansatz describes a spin-$\frac{1}{2}$ fermion, and these two fermions possess the same masses $\mu$ and opposite spins. Although the energy-momentum tensors of these fermions are not spherically symmetric, their sum provides a spherically symmetric energy-momentum tensor.

Converting the Ansatz (9) into spherical coordinates (see Ref. [18]) and substituting the resulting expression and the metric (8) into the field equations (3), (4), and (6), one can obtain the following set of equations:

$$A'' + \left(\frac{2x}{x^2+x_0^2} + \frac{1}{2}\frac{B'}{B}\right)A' + 2e^{-3A/2}B\left[e^{A/2}(\bar{u}^2-\bar{v}^2) - 2\bar{\Omega}(\bar{u}^2+\bar{v}^2)\right] = 0, \tag{10}$$

$$B'' + \left(\frac{3x}{x^2+x_0^2} - \frac{1}{2}\frac{B'}{B}\right)B' + 4e^{-\frac{A}{2}}B^{\frac{3}{2}}\frac{\bar{u}\bar{v}}{\sqrt{x^2+x_0^2}} + 4e^{-3A/2}B^2\left[e^{A/2}(\bar{u}^2-\bar{v}^2) - \bar{\Omega}(\bar{u}^2+\bar{v}^2)\right] = 0, \tag{11}$$

$$\bar{u}' + \left(\frac{x}{x^2+x_0^2} - \frac{1}{\sqrt{x^2+x_0^2}} - \frac{1}{4}A' + \frac{1}{2}\frac{B'}{B}\right)\bar{u} + e^{-A}\sqrt{B}\left(\bar{\Omega}+e^{A/2}\right)\bar{v} = 0, \tag{12}$$

$$\bar{v}' + \left(\frac{x}{x^2+x_0^2} + \frac{1}{\sqrt{x^2+x_0^2}} - \frac{1}{4}A' + \frac{1}{2}\frac{B'}{B}\right)\bar{v} - e^{-A}\sqrt{B}\left(\bar{\Omega}-e^{A/2}\right)\bar{u} = 0, \tag{13}$$

$$\left[\sqrt{B}(x^2+x_0^2)\bar{\phi}'\right]' = 0, \tag{14}$$

where the prime denotes differentiation with respect to the radial coordinate. Here, Eq. (10) is derived from the Einstein equations (3) as the combination $[(\,^t_t) - (\,^r_r)]$, where the second derivative $B''$ is excluded using the $(\,^\theta_\theta)$-component. In turn, Eq. (11) is the combination $\left[(\,^r_r) + (\,^\theta_\theta)\right]$. The above equations are written in terms of the following dimensionless variables and parameters:

$$x = \mu r, \quad \bar{\Omega} = \frac{\Omega}{\mu}, \quad (\bar{u},\bar{v}) = \sqrt{\frac{4\pi G}{\mu}}(u,v), \quad \bar{\phi} = \sqrt{8\pi G}\phi. \tag{15}$$

Note that Eqs. (10) and (11) do not contain the scalar field explicitly, since it can be eliminated by combining the corresponding components of the Einstein equations. In turn, the integration of the scalar field equation (14) yields

$$\bar{\phi}' = \frac{\sqrt{\bar{D}}}{\sqrt{B}(x^2+x_0^2)}, \tag{16}$$

where the dimensionless integration constant $\bar{D} \equiv 8\pi G\mu^2 D$ represents the scalar charge of the ghost field. By substituting this expression into the $(\,^r_r)$-component of the Einstein equations (3), one can find

$$\bar{D} = -\frac{1}{2}(x^2+x_0^2)^2\frac{B'^2}{B} - 2x(x^2+x_0^2)B' + \frac{1}{2}[4x_0^2 + (x^2+x_0^2)^2A'^2]B + 4e^{-\frac{3A}{2}}(x^2+x_0^2)^2B^2\left[\bar{\Omega}(\bar{u}^2+\bar{v}^2) - e^{\frac{A}{2}}(\bar{u}^2-\bar{v}^2)\right] - 8e^{-A/2}(x^2+x_0^2)^{3/2}B^{3/2}\bar{u}\bar{v}. \tag{17}$$

Below we use the condition $\bar{D} = \text{const}$ to check the quality of the numerical solutions. The variation of the constant $\bar{D}$ as calculated from Eq. (17) is typically less than $10^{-4}$.

## 3. Numerical solutions

In this section, we solve numerically the equations (10)-(14) and compare the physical properties of the configurations obtained.

### *3.1 Asymptotic behavior and boundary conditions*

We seek regular solutions of the set of five ordinary differential equations (10)-(14) possessing finite energy. Even before numerical solving these equations, it is possible to estimate an asymptotic behavior of the solutions bearing in mind that the functions $\bar{u}$ and $\bar{v}$ should decay exponentially with distance as $x \to \pm\infty$. It is seen from the form of Eqs. (12) and (13) that, due to the presence of the term $(x^2 + x_0^2)^{-1/2}$, they are not $Z_2$-symmetric. This implies that we should seek solutions that are asymmetric with respect to the origin of coordinates $x = 0$. Then the corresponding asymptotic behavior of the spinor fields has the form

$$\bar{u} \approx \bar{u}_{\pm\infty} \frac{e^{\mp\sqrt{1-\bar{\Omega}^2}x}}{x} + \cdots, \quad \bar{v} \approx \bar{v}_{\pm\infty} \frac{e^{\mp\sqrt{1-\bar{\Omega}^2}x}}{x} + \cdots,$$

where $\bar{u}_{\pm\infty}, \bar{v}_{\pm\infty}$ are integration constants for $x \to \pm\infty$, respectively. In turn, for the metric functions $A$ and $B$, one can find from Eqs. (10) and (11) as $x \to \pm\infty$

$$A \approx \mp\frac{2\bar{M}_{\pm}}{x} + \cdots, \quad B \to 1 + \cdots. \tag{18}$$

In this formula $\bar{M}_+$ corresponds to a total mass of the configurations under consideration as measured by a distant observer when $x \to +\infty$ and $\bar{M}_-$ is the mass as measured when $x \to -\infty$.

Eq. (16) implies the following asymptotic behavior of the scalar field:

$$\bar{\phi} \approx \bar{\phi}_{\pm\infty} - \frac{\sqrt{\bar{D}}}{x} + \cdots,$$

where $\bar{\phi}_{\pm\infty}$ are two integration constants corresponding to the values of the scalar field as $x \to \pm\infty$, respectively.

Taking into account the asymptotic behavior given above, the corresponding boundary conditions can be taken in the form

$$A(x \to \pm\infty) = 0, \quad B(x \to \pm\infty) = 1,$$
$$\bar{u}(x \to \pm\infty) = 0, \quad \bar{v}(x \to \pm\infty) = 0, \quad \bar{\phi}(x \to \pm\infty) = \bar{\phi}_{\pm\infty}. \tag{19}$$

These boundary conditions imply that we are dealing with asymptotically flat spacetime.

### *3.2 Numerical method*

We solve the system of mixed order differential equations (10)-(14) using the boundary conditions (19) and the constraint equation (17) to verify the accuracy of calculations.

In order to map the infinite range of the radial variable $x$ to the finite interval, we employ the compactified coordinate $\bar{x}$,

$$\bar{x} = \frac{2}{\pi}\arctan\left(\frac{x}{c_k}\right), \tag{20}$$

which maps the infinite region $(-\infty; \infty)$ onto the finite interval $[-1; 1]$. Here $c_k$ is a constant which is used to adjust the contraction of the grid. In our calculations, we typically take $c_k \in [0.1,3]$.

Technically, Eqs. (10)-(14) are discretized on a grid consisting of about 1000 grid points. The resulting system of nonlinear algebraic equations is then solved by using a modified Newton method. The underlying linear system is solved with the Intel MKL PARDISO sparse direct solver [19] and the CESDSOL library (Complex Equations-Simple Domain partial differential equations SOLver, a C++ package developed by I. Perapechka, see Refs. [20, 21]). The package provides an iterative procedure to obtain an exact solution starting from some initial guess configuration.

*3.3 Mass and the circumferential radius*

We consider Dirac-star-plus-wormhole configurations that are asymptotically flat and asymmetric with respect to the center $x = 0$. The important point here is the behavior of the circumferential radius $\bar{R}(x)$ which is defined as

$$\bar{R}^2 \equiv g_{\theta\theta} = Be^{-A}(x^2 + x_0^2). \tag{21}$$

Asymptotic flatness implies that $\bar{R}(x) \to |x|$ for large $|x|$. Due to the asymmetry of the configurations, the center of the systems located at $x = 0$ should not in general be an extremum of $\bar{R}(x)$. Depending on the concrete values of the system parameters, the extremum of $\bar{R}(x)$ can be situated both to the left and to the right of the point $x = 0$. If $\bar{R}(x)$ has only one global minimum at some point $x = x_{\rm extr}$, then $x_{\rm extr}$ is the throat of the wormhole $\bar{R}_{\rm th} = \min\{\bar{R}(x)\}$ (a single-throat system). If, on the other hand, $\bar{R}(x)$ has a local maximum at $x = x_{\rm extr}$, then this point is an equator $\bar{R}_{\rm eq} = \max\{\bar{R}(x)\}$. This then implies that there are (at least) two minima of $\bar{R}(x)$ (on account of the asymmetry of the system, one of them is global and another one – local), located, in general, asymmetrically to the left and to the right of the maximum. In the case of two such minima, the wormhole under consideration will have a double throat (see, e.g., Refs. [9, 22, 23]).

Let us now turn to the total mass of the systems under consideration. Since they are asymmetric with respect to the center $x = 0$, a distant observer placed at $x \to \pm\infty$ measures different magnitudes of the mass $\bar{M}_+$ and $\bar{M}_-$ at infinity, see Eq. (18). They correspond to a dimensionless ADM (Arnowitt-Deser-Misner) mass of the system $\bar{M}$ given by

$$\bar{M}_\pm \equiv \mu M_\pm / M_p^2 = \pm\frac{1}{2}\lim_{x\to\pm\infty} x^2\,\partial_x e^A = \pm\frac{c_k}{\pi}\lim_{\bar{x}\to\pm 1}\partial_{\bar{x}} A, \tag{22}$$

where $M_p$ is the Planck mass and the last expression in the above equation represents the mass in terms of the compactified coordinate $\bar{x}$ from Eq. (20).

Alternatively, the mass of the configuration may also be found from the $\binom{t}{t}$-component of the energy-momentum tensor (7),

$$m(r) = \frac{1}{2G}R_{\rm extr} + 4\pi\int_{R_{\rm extr}}^{r} T_t^t R^2 dR. \tag{23}$$

In this expression, the circumferential radius $R_{\rm extr}$ corresponds either to the radius of the wormhole throat $R_{\rm th}$ (for single-throat systems) or to the radius of the equator $R_{\rm eq}$ (for double-throat systems). In terms of the dimensionless variables (15) the formula (23) can be represented in the form

$$\bar{m}(x) \equiv G\mu m(r) = \frac{\bar{R}_{\rm extr}}{2} + \frac{1}{4}\int_{x_{\rm extr}}^{x} \bar{T}_t^t \bar{R}^2 \frac{d\bar{R}}{dx'}\,dx', \tag{24}$$

where $x_{\rm extr}$ is the point on the $x$-axis where a throat or an equator are situated. The expression (24) can be used to monitor the accuracy of the numerical calculations.

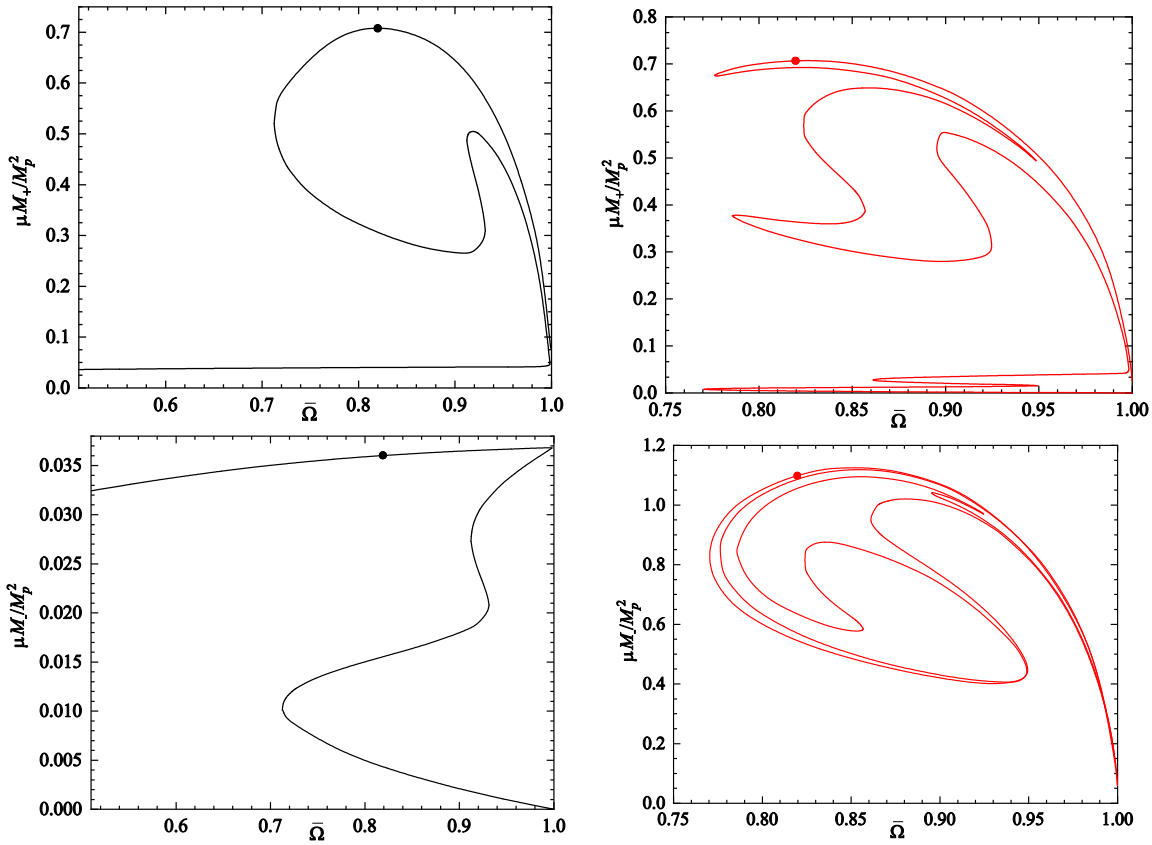


**Figure 1.** The dimensionless Dirac-star-plus-wormhole total mass $\bar{M}_{\pm}$ as a function of the parameter $\bar{\Omega}$ for $x_0 = 0.03$ for two different families of solutions.

*3.4 Numerical results*

Using the boundary conditions (19), we solve a two-point boundary value problem for the system of equations (10)-(14). This system can be solved for different values of the free parameters $x_0$ and $\bar{\Omega}$ to obtain regular solutions.

Solutions of the set of equations (10)-(14) have already been studied earlier in Ref. [13]. There were obtained solutions for different values of the throat parameter $x_0$ and constructed the dependencies of the total mass of the system on the frequency $\bar{\Omega}$. Here we extend those solutions by new results for the case of $x_0 = 0.03$ which are absent in Ref. [13]. This enables us to compare this extended family of solutions with another family found in Ref. [14] and to demonstrate a qualitatively different behavior of dependencies of the total mass on the spinor frequency. Namely, Fig. 1 shows the dependencies of the masses $\bar{M}_+$ and $\bar{M}_-$ on the frequency $\bar{\Omega}$ for the two aforementioned families of solutions for a fixed $x_0 = 0.03$.

The family of solutions shown in the left panels of Fig. 1 is characterized by the fact that the solutions start at $\bar{\Omega} = 1$ from the limiting Ellis wormhole solution with zero mass. However, as the frequency $\bar{\Omega}$ gradually decreases, there is some limiting value $\bar{\Omega}_1 < 1$, for which one can still perform numerical calculations. It is important to note that when the frequency tends to $\bar{\Omega}_1$, the metric function $g_{tt} \equiv e^A \to 0$. The latter assumes the possible presence of a horizon for such

systems. Moreover, in this limit, the dimensionless Kretschmann scalar $\overline{K} \equiv K/\mu^4 = \bar{R}_{\alpha\beta\mu\nu}\bar{R}^{\alpha\beta\mu\nu}$ diverges, i.e., such systems possess a singularity – a possible singular horizon. Note also that in this case we deal with a double-throat system.

In turn, the family of solutions shown in the right panels of Fig. 1 is characterized by a different in principle qualitative behavior. Here, as in the case of the first family, the solutions start at $\overline{\Omega} = 1$ from the limiting Ellis wormhole solution with zero mass. However, this family is characterized by a considerably more complicated structure of branches with large number of turning points. Eventually, unlike the solutions of the first family, here the solutions return back to the starting point $\overline{\Omega} = 1$. In this case, the Kretschmann scalar remains always finite, i.e., the configurations under consideration are always regular, in contrast to the systems from the first family of solutions when a fast increase of $\overline{K}$ for $\overline{\Omega} \to \overline{\Omega}_1$ occurs.

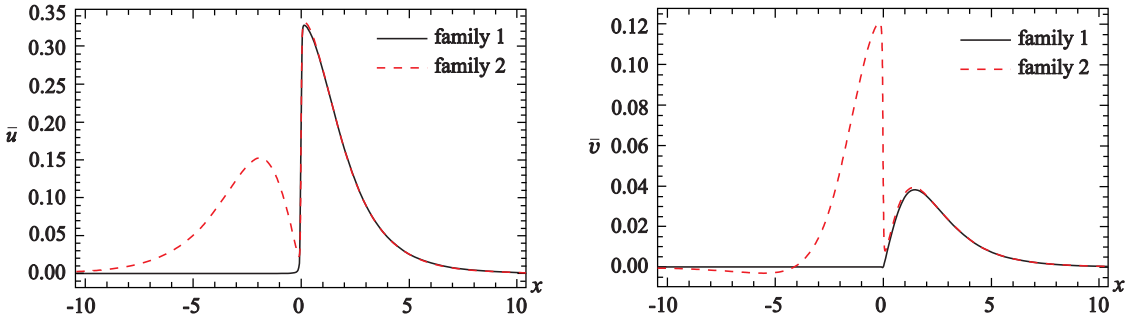


**Figure 2.** Typical solutions for the spinor fields for the configurations marked by the bold dots in Fig. 1.

The aforementioned strong differences in the behavior of the mass curves are caused by qualitative differences in the behavior of the solutions for the two families under consideration. To illustrate this, we show in Fig. 2 the characteristic behavior of the spinor fields $\bar{u}$ and $\bar{v}$ for two families of solutions with one frequency $\overline{\Omega} = 0.82$ (the corresponding configurations are marked by the bold dots in the mass curves in Fig. 1). It is seen from these graphs that, for the configurations from the first family (the left panels of Fig. 1), the spinor fields are concentrated to the right of the center of the system, while the spinor fields are small to the left of the center. This results in the fact that for such systems the total mass $\overline{M}_+ \gg \overline{M}_-$. On the other hand, for the configurations from the second family (the right panels of Fig. 1), the spinor fields have comparable values to the right and to the left of the center $x = 0$. As a result, the total masses of such systems $\overline{M}_+$ and $\overline{M}_-$ are comparable in magnitude as well.

## 4. Conclusion

In the present paper, we have considered a mixed system consisting of a wormhole threaded by a spinor field. A nontrivial wormhole-type topology in the system is provided by a massless ghost scalar field. For such a mixed system, we have constructed families of regular asymptotically flat solutions for explicitly time-dependent spinor fields, oscillating with a frequency Ω. The resulting mixed configurations are asymmetric with respect to the center, in contrast to all mixed systems considered by us earlier [6-12, 24] . The characteristics of the systems thus obtained that are observed at two asymptotic ends of a wormhole (that is, as $r \to \pm\infty$) may differ considerably.

For the field system under consideration, there are two families of solutions which differ considerable both in the behavior of the mass curves and in physical characteristics. Namely, the first family is characterized by the concentration of the mass to the right of the center of the system when $\bar{M}_+ \gg \bar{M}_-$ in the wide range of frequencies Ω. In this case, as one moves along the mass curve with decreasing Ω, there is a fast increase in the spacetime curvature; this eventually may lead to forming a singular horizon at some limiting $\bar{\Omega}$ not equal to 0 or 1. In turn, the configurations of the second family are characterized by a very complicated structure of the branches of the mass curve with large number of turning points. However, in contrast to the configurations of the first family, for the systems of the second family, there are no any limiting values of $\bar{\Omega}$ where a singularity might occur: the solutions are regular for all allowed values of the frequency.

## Acknowledgements

This research was funded by the Committee of Science of the Ministry of Science and Higher Education of the Republic of Kazakhstan (Grant No. BR21881941 "Experimental and theoretical research in the field of high and ultrahigh energies for solving urgent problems of astrophysics and cosmic ray physics").

## References

[1] Amendola L. and Tsujikawa S. Dark Energy: Theory and Observations. - Cambridge University Press, Cambridge, England, 2010. – 491 p.
[2] Ade P. A. R. et al. [Planck Collaboration] Planck 2015 results. XIII. Cosmological parameters // Astron. Astrophys. – 2016. – V. A13. – P. 594.
[3] Bronnikov K. A. Scalar-tensor theory and scalar charge // Acta Phys. Polon. – 1973. – V. B4. – P. 251.
[4] Ellis H. G. Ether flow through a drainhole - a particle model in general relativity // J. Math. Phys. – 1973. – V. 14. – P. 104.
[5] Ellis H. G. The Evolving, Flowless Drain Hole: A Nongravitating Particle Model In General Relativity Theory // Gen. Rel. Grav. – 1979. – V.10. – P. 105.
[6] Dzhunushaliev V., Folomeev V., Kleihaus B., and Kunz J. A star harbouring a wormhole at its core // J. Cosmol. Astropart. Phys. – 2011. – V. 04:031. – 21 p.
[7] Dzhunushaliev V., Folomeev V., Kleihaus B., and Kunz J. Mixed neutron star-plus-wormhole systems: Equilibrium configurations // Phys. Rev. – 2012. – V. D85:124028. -14 p.
[8] Dzhunushaliev V., Folomeev V., Kleihaus B., and Kunz J. Mixed neutron-star-plus-wormhole systems: Linear stability analysis // Phys. Rev. – 2013. – V. D87:104036. – 12 p.
[9] Dzhunushaliev V., Folomeev V., Kleihaus B., and Kunz J. Hiding a neutron star inside a wormhole// Phys. Rev. – 2014. – V. D89:084018. – 14 p.
[10] Aringazin A., Dzhunushaliev V., Folomeev V., Kleihaus B., and Kunz J. Magnetic fields in mixed neutron-star-plus-wormhole systems // J. Cosmol. Astropart. Phys. – 2015. – V. 04:005. -22 p.
[11] Dzhunushaliev V., Folomeev V., and Urazalina A. Star-plus-wormhole systems with two interacting scalar fields // Int. J. Mod. Phys. – 2015. – V. D24:1550097. -15 p.
[12] Dzhunushaliev V., Folomeev V., Kleihaus B., and Kunz J. Can mixed star-plus-wormhole systems mimic black holes? // J. Cosmol. Astropart. Phys. – 2016. – V.08:030. – 26 p.
[13] Hao C. H., Sun S. X., Huang L. X., Zhang R., Su X., and Wang Y. Q. Dirac stars in wormhole spacetime // JCAP – 2024. – V.04, 057. – 27 p.
[14] Dzhunushaliev V., Folomeev V. and Sakhiyev S. Dirac stars with wormhole topology // [arXiv:2505.05818 [gr-qc]].
[15] Lawrie I. A Unified Grand Tour of Theoretical Physics. - Institute of Physics Publishing, Bristol, 2002. -565 p.
[16] Soler M. Classical, stable, nonlinear spinor field with positive rest energy // Phys. Rev. – 1970. – V. D1. - P. 2766.
[17] Herdeiro C. A. R., Pombo A. M., and Radu E. Asymptotically flat scalar, Dirac and Proca stars: discrete vs. continuous families of solutions // Phys. Lett. – 2017. – V. B773. – P. 654.

[18] Dzhunushaliev V. and Folomeev V. Dirac stars supported by nonlinear spinor fields // Phys. Rev. – 2019. – V. D99:084030. – 7 p.
[19] Gould N.I.M., Scott J.A., Hu Y. A numerical evaluation of sparse direct solvers for the solution of large sparse symmetric linear systems of equations // ACM Trans. Math. Softw. – 2007. – V. 33. – P. 10.
[20] Herdeiro C., Perapechka I., Radu E., and Shnir Y. Asymptotically flat spinning scalar, Dirac and Proca stars // Phys. Lett. – 2019. – V. B797:134845. – 8 p.
[21] Herdeiro C., Perapechka I., Radu E., and Shnir Y. Spinning gauged boson and Dirac stars: A comparative study // Phys. Lett. – 2022. – V. B824:136811. – 7 p.
[22] Charalampidis E., Ioannidou T., Kleihaus B., and Kunz J. Wormholes threaded by chiral fields // Phys. Rev. – 2013. – V. D87:084069. – 12 p.
[23] Hauser O., Ibadov R., Kleihaus B., and Kunz J. Hairy Wormholes and Bartnik-McKinnon Solutions // Phys. Rev. – 2014. – V. D89:064010. – 11 p.
[24] Dzhunushaliev V., Folomeev V., Kleihaus B., and Kunz J. Mixed neutron-star-plus-wormhole systems: Rotating configurations // Phys. Rev. – 2023. – V. D107:044060. – 9 p.